Rydberg and valence excited states of dibromomethane in 35,000–95,000 cm−1 region studied using synchrotron radiation

ARTICLE *in* JOURNAL OF QUANTITATIVE SPECTROSCOPY AND RADIATIVE TRANSFER · SEPTEMBER 2014

Impact Factor: 2.65 · DOI: 10.1016/j.jqsrt.2014.04.005

Journal of Quantitative Spectroscopy & Radiative Transfer 144 (2014) 164–173

Contents lists available at ScienceDirect

Journal of Quantitative Spectroscopy & Radiative Transfer

journal homepage: www.elsevier.com/locate/jqsrt

Rydberg and valence excited states of dibromomethane in 35,000–95,000 cm^{-1} region studied using synchrotron radiation

Anuvab Mandal [a], Param Jeet Singh [b,*], Aparna Shastri [b], Vijay Kumar [c], B.N. Raja Sekhar [b], B.N. Jagatap [a]

[a] Homi Bhabha National Institute, Mumbai 400094, India
[b] Atomic and Molecular Physics Division, BARC, Trombay, Mumbai 400085, India
[c] Indus Operation and Accelerator Physics Development Division, RRCAT, Indore, India

ARTICLE INFO

Article history:
Received 28 November 2013
Received in revised form
9 April 2014
Accepted 14 April 2014
Available online 19 April 2014

Keywords:
Dibromomethane
Vacuum ultraviolet spectrum
Rydberg series
Valence states
TDDFT calculation
Synchrotron radiation

ABSTRACT

The UV–VUV photoabsorption spectrum of dibromomethane (CH_2Br_2) in the energy region 4.3–11.8 eV (35,000–95,000 cm^{-1}) is investigated using synchrotron radiation. Rydberg series converging to the first four ionization limits at 10.52, 10.74, 11.21 and 11.30 eV corresponding to excitations from the $3b_1$, $2b_2$, $1a_2$, and $4a_1$ orbitals of CH_2Br_2 are identified and analyzed. Quantum defect values are observed to be consistent with excitation from the bromine lone pair orbitals. Assignments of the *ns* Rydberg series are revised and the *np* and *nd* Rydberg series are assigned for the first time. Observed vibrational features accompanying the 5*p* and 4*d* Rydberg states are assigned exclusively to the totally symmetric (a_1) –CBr symmetric stretching mode (ν_3) in contrast to the earlier assignment to ν_3 and $-CH_2$ bending (ν_2) modes. The Rydberg and valence transitions observed in the present experiment are found to be in good agreement with the vertical excited states calculated using the TDDFT method. The calculations are further used to infer the valence transitions responsible for the broad intensity pedestals underlying the Rydberg transitions. The assignments are confirmed using isotopic substitution studies on CD_2Br_2 whose UV–VUV photoabsorption spectrum is reported here for the first time. This work presents a consolidated analysis of the UV–VUV photoabsorption spectrum of dibromomethane.

1. Introduction

Dibromomethane (CH_2Br_2) is produced in seawater by macroalgae and released into the atmosphere by volatilization [1]. In the troposphere, it degrades by reacting with the hydroxyl (OH) radical which is produced by photolysis of ozone, thereby playing an important role in the ozone balance in the atmosphere [2,3]. A recent study on global modeling of CH_2Br_2 has indicated that CH_2Br_2 plays an important role in contributing reactive bromine to the stratosphere [4]. Vacuum ultraviolet (VUV) photoabsorption studies of dihalomethanes are important in the understanding of dissociation channels [5] and associated complex photochemical reactions of CH_2Br_2 in atmosphere and interstellar space [4]. Several photodissociation studies using techniques such as photoelectron photoion coincidence (PEPICO) [5,6], ion velocity imaging [7,8], resonance enhanced multiphoton ionization [9], laser induced [10] and cavity ring down spectroscopy [11] have been reported

* Corresponding author. Tel.: +91 22 2559 2995; fax: +91 22 2550 2652.
E-mail address: singhp@barc.gov.in (P.J. Singh).

http://dx.doi.org/10.1016/j.jqsrt.2014.04.005
0022-4073/

previously. The first few ionization potentials (*IPs*) of CH_2Br_2 are known from PEPICO [5,6], photoelectron spectroscopy (PES) [12,13] and Penning ionization electron spectroscopy [12]. Ultraviolet absorption cross sections of CH_2Br_2 at room temperature were measured by Molina et al. [3] and the temperature-dependent study was carried out by Gillottay and co-workers [14]. Mossinger et al. [2] reported UV–visible absorption cross section over a range of temperatures and estimated the atmospheric life time of CH_2Br_2. Recently, Liu et al. have performed spin orbit ab initio calculations for photodissociation of CH_2Br_2 [15].

The VUV absorption spectrum of CH_2Br_2 was reported for the first time using hydrogen discharge lamp by Causley and Russell in 1975 [16]. Many of the observed lines were assigned to *ns* (up to $n=9$) Rydberg series converging to three *IP*s, viz., b_1, b_2 and (a_1+a_2) and the first members of *np* and *nd* Rydberg transitions were assigned based on term value calculations. In their work several observed peaks were left unassigned and a few features were given tentative assignments. To the best of our knowledge, there is no other experimental photoabsorption study of CH_2Br_2 in the VUV region; also the related theoretical studies are restricted to the UV region [9,15]. Thus a complete understanding of the UV–VUV spectrum of CH_2Br_2 is still lacking.

In this paper we report UV–VUV spectroscopy of dibromomethane in the energy region of4.3–11.8 eV using synchrotron radiation. A complete Rydberg series and vibronic analysis is carried out to build a better understanding of the high-lying excited states of CH_2Br_2. The analysis is further supported by performing quantum chemical calculations in DFT and TDDFT framework. The work has resulted in assignments of observed spectrum of CH_2Br_2 to *ns*, *np* and *nd* Rydberg series converging to four *IP*s. Proposed assignments are confirmed and consolidated by the UV–VUV photoabsorption spectrum of the deuterated species, diboromomethane-d_2 (CD_2Br_2), whose spectrum is reported here for the first time.

2. Experimental

Photoabsorption experiments were performed in the energy region of 3.5-11.8 eV (1050-3500 Å) at an average resolving power of ~1000 using monochromatic synchrotron radiation from the photophysics beamline at 450 MeV storage ring Indus-1, Raja Ramanna Centre for Advanced Technology, Indore, India. A 250 mm long single-pass stainless steel gas cell was used in these experiments. The cell was evacuated to a base pressure of $\sim 10^{-6}$ mbar. Samples of CH_2Br_2 and CD_2Br_2, (M/s. Sigma Aldrich) with stated purities $>99.5\%$, were purified by repeated freeze-pump-thaw cycles and filled in the cell at various pressures in the range from 10^{-4} to 1 mbar as measured using absolute capacitance gauges (M/s. Pfeiffer make). Transmitted intensities were detected using a UV–visible sensitive photomultiplier tube coupled with a sodium salicylate coated quartz window. The spectrum was recorded and further normalized w.r.t. the synchrotron beam current which is recorded concurrently with a step size of 0.5 Å, corresponding to 13 cm^{-1} at 50,000 cm^{-1} and 41 cm^{-1} at 90,000 cm^{-1}, which decides the precision of the measurement. Absorption spectrum was generated, in accordance with the Beer–Lambert law, by plotting $\ln(I_0/I)$ vs. wavelength where I_0 and I are normalized intensities without and with the sample, respectively. The atomic absorption lines of xenon were used as a reference to calibrate the wavelength scale. Using this method, the overall error in determination of line positions is found to be within the experimental resolution. Details of the beamline [17] and the experimental setup may be found in our earlier publications [18–20].

3. Computational

The aim of the calculation is to generate the excited state energies for comparison with the experimentally observed photoabsorption spectrum. CH_2Br_2 is a 78 valence electron system having C_{2v} geometry in the ground state. The molecular orbital configuration of CH_2Br_2 is given as $[core](1a_1)^2(1b_1)^2(2a_1)^2(1b_2)^2(3a_1)^2(2b_1)^2(4a_1)^2(1a_2)^2(2b_2)^2(3b_1)^2$: X^1A_1. The coordinate system used is such that the H–C–H group of CH_2Br_2 molecule lies in *YZ* plane and Br–C–Br in *XZ* plane as shown in Fig. 1. All the electronic structure calculations are performed using the GAMESS (US) computational chemistry code [21] on a LINUX-based cluster platform. Knowledge of vibrational frequencies of ground state and excited states are important for the analysis of observed absorption spectra. The ground state geometry of CH_2Br_2 and CD_2Br_2 are optimized and the vibrational frequencies are calculated using the density functional theory (DFT) and Møller-Plesset perturbation theory (MP2) with different basis sets. Electron correlation in the DFT calculation is included by the use of hybrid exchange correlation functionals, viz., Becke–3–Lee–Yang–Parr (B3LYP) [22,23] and Perdew–Burke–Ernzerhof (PBE0) [24]. Ground state bond lengths, bond angles and normal mode frequencies are calculated using several basis sets including Pople's split valence basis set 6-31G with d- and f-type polarization functions [25,26], which are known to be suitable for recovering the correlation energy. Since experimentally observed vibrational frequencies of Rydberg states of a molecule can be approximated by its ionic ground state frequencies [18–20], the

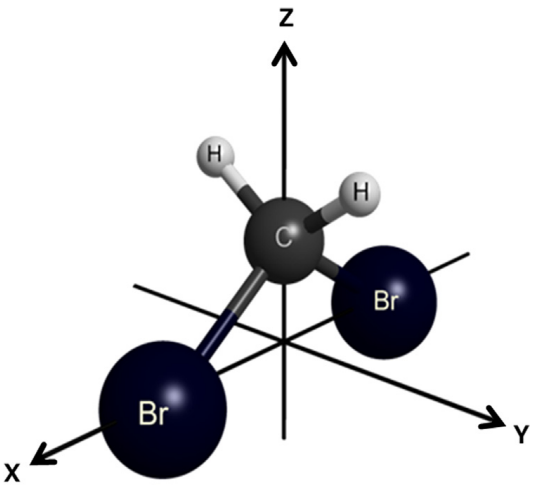

Fig. 1. Geometry of CH_2Br_2 under C_{2v} symmetry.

ground states of the ions $CH_2Br_2^+$ and $CD_2Br_2^+$ are also optimized and their vibrational frequencies are calculated. The calculated geometries of the ground state and vibrational frequencies of CH_2Br_2 and CD_2Br_2 for both neutral and ionized molecules at PBE0/aug-cc-pV5Z level are shown in Tables 1 and 2. Theoretical results obtained using PBE0 energy functional are in better agreement than B3LYP with the experimental values wherever available [5,27,28]. The vibrational frequencies are also compared with theoretical calculations reported earlier [29,30]. Analysis of vibronic features in the experimental electronic absorption spectra is aided by these computed values. Here we note that since the four highest occupied molecular orbitals correspond to Br lone pair type and are similar in shape, equilibrium geometries and vibrational frequencies of the ionic states corresponding to removal of an electron from each of these MOs are not expected to differ much. Hence only the lowest ionic state has been optimized and resultant vibrational frequencies used as a guideline in the analysis.

The vertical excited state energies of CH_2Br_2 are calculated using the time-dependent density functional theory (TDDFT) at the optimized geometry of the ground state, using correlation functionals B3LYP and PBE0 with various basis sets, viz., cc-pV*n*Z and aug-cc-pV*n*Z, (n = D, T, Q, 5). Of these functionals/basis sets used, the PBE0/aug-cc-pV5Z combination is found to yield better results in terms of agreement with experimental values. The calculations are restricted to the excited states below 12 eV since the region of interest is 3.5–11.8 eV. About 100 singlet excited states below 12 eV are predicted by the calculations but only a few of them have appreciable oscillator strengths. The Λ diagnostic value which is a measure of the spatial overlap in a given excitation [31] is also calculated for all the excited states. In general $\Lambda \leq 0.3$ indicates Rydberg type transitions while $\Lambda \geq 0.6$ indicates valence type transitions. Intermediate values of Λ signify valence-Ryberg mixed type transitions. TDDFT calculations greatly aid in the assignment as is discussed in what follows.

Table 1
Optimized geometry parameters (bond length in Å and angle in deg) for neutral and ionized dibromomethane using PBE0/aug-cc-pV5Z.

Parameter	CH_2Br_2		$CH_2Br_2^+$
	Present study	Expt. [28]	Present study
***r*(C–Br)**	1.922	1.925	1.921
***r*(C–H)**	1.083	1.097	1.084
∠Br–C–Br	113.7	112.9	92.6
∠H–C–Br	107.8	108.3	111.3
∠H–C–H	112.0	110.9	116.5

4. Results and discussions

The photoabsorption spectra of CH_2Br_2 and CD_2Br_2 in the region of 35,000-95,000 cm^{-1} (~4.3-11.8 eV) recorded using the photophysics beamline at Indus-1 are shown in Fig. 2, in both wavenumber and energy scales. The spectrum is quite structured and is divided into five energy regions (1) 4.3-6.7 eV with two broad features, (2) 6.8-7.8 eV with four diffuse bands, (3) 7.8-8.7 eV with sharp structure, (4) 8.6-9.6 eV with intense peaks and (5) > 9.7 eV with diffuse peaks. Note here that regions (1)–(4) are as per the nomenclature of Causley et al. [16] while region (5) is additionally observed in our work. Most of the transitions observed in the VUV region are of Rydberg type, with several valence transitions contributing to the overall intensity. Rydberg series analysis, assignment of vibrational features and contribution of valence transition and their interpretation with theoretical calculations are discussed in what follows.

4.1. Rydberg series

In the energy region 6.0-11.0 eV extensive Rydberg series converging to the first four ionization limits of CH_2Br_2 are observed (c.f. Fig. 2). The highest four occupied molecular orbitals (MO) of CH_2Br_2 ($3b_1$, $2b_2$, $1a_2$, $4a_1$) are of non-bonding type and they correspond to bromine lone pair orbitals. The ordering of the four highest occupied MOs in early PES studies has been rather controversial, i.e., $3b_1$, $2b_2$, $1a_2$, $4a_1$ by Dixon et al. [12] and Kishimoto et al. [13] and $2b_2$, $1a_2$, $3b_1$, $4a_1$ by Potts et al. [32]. The present quantum chemical calculation clearly shows the order to be $3b_1$, $2b_2$, $1a_2$, $4a_1$ and is confirmed by repeating the calculations for several basis sets and methods. The first four*IPs* arising from the removal of an

Table 2
Calculated (PBE0/aug-cc-pV5Z) and reported ground state frequencies (in cm^{-1}) for neutral and ionized dibromomethane.

Normal mode (symmetry)	Neutral dibromomethane				Ionic dibromomethane		
	CH_2Br_2		CD_2Br_2		$CH_2Br_2^+$		$CD_2Br_2^+$
	This work	Expt. [27]	This work	Expt. [27]	This work	Calc. [5]	This work
ν_1: CH sym. stretch (a_1)	3143	3009	2278	2196	3140	3141	2272
ν_2: CH_2 bend (a_1)	1432	1382	1051	1027	1424	1438	1046
ν_3: CBr sym. stretch (a_1)	599	588	570	550	669	619	636
ν_4: CBr_2 bend (a_1)	171	169	170	172	180	162	179
ν_5: CH_2 twist (a_2)	1123	1095	796	784	1040	1053	738
ν_6: CH_2 wag (b_1)	1217	1195	916	901	1175	1202	887
ν_7: CBr asym. stretch (b_1)	668	653	629	610	578	527	550
ν_8: CH asym. stretch (b_2)	3231	3073	2406	2313	3255	3234	2429
ν_9: CH_2 rock (b_2)	806	812	635	636	888	883	681

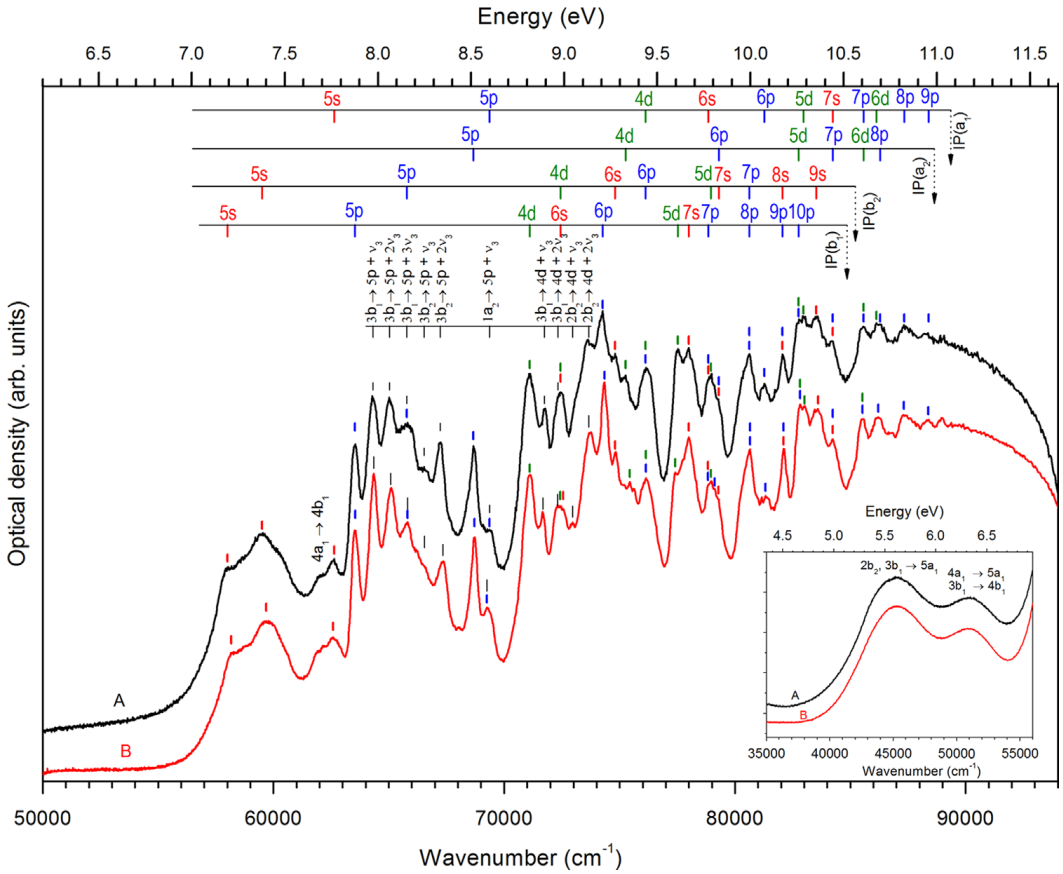

Fig. 2. UV–VUV photoabsorption spectra of CH_2Br_2 (curve A) and CD_2Br_2 (curve B) showing Rydberg series converging to first four ionization potentials (*IP*) at 10.52 (b_1), 10.74 eV (b_2), 11.21 eV (a_2) and 11.30 eV (a_1). Spectra are recorded at sample pressure of 0.06 mbar. Inset shows low energy spectra (4.3–6.8 eV) at high sample pressure (~1 mbar). Vibronic features accompanying 5*p* ($3b_1$, $2b_2$ and $1a_2$) and 4*d* ($3b_1$ and $2b_2$) states are also marked.

electron from these orbitals are 10.52, 10.74, 11.21 and 11.30 eV [13]. It may be noted that these *IP*s are quite closely spaced, particularly the third and fourth.

The observed UV–VUV absorption spectrum is due to transitions from non-bonding orbitals into the first few unoccupied orbitals. The Rydberg series can be fitted to the well-known Rydberg formula: $E_n = IP - R/(n-\delta_l)^2$ where E_n is the energy of the transition, *IP* is the ionization potential, *R* is the Rydberg constant, *n* is the principal quantum number and δ_l is the quantum defect, *l* being the angular momentum. Using this expression Rydberg series of *ns*, *np* and *nd* type converging to first four *IP*s of CH_2Br_2 and CD_2Br_2 are identified; see Table 3 for peak positions and quantum defects.

The *ns* orbitals are expected to have a_1 symmetry, therefore transitions from $1a_2 \rightarrow ns$ are forbidden due to symmetry selection rules for C_{2v} point group and expected to have zero oscillator strength. Consequently *ns* series are observed only for *IP*s corresponding to b_1, b_2 and a_1 while *np* and *nd* series are observed for all four *IP*s. In each Rydberg series we define n_{max} as the maximum value of *n*. In *ns* series for transition from $2b_2$, $3b_1$, $4a_1 \rightarrow ns$, $n_{max}=9$, 7, 7, respectively. In case of *np* Rydberg series, $n_{max}=10$, 7, 8, 9 is observed corresponding to the transitions $3b_1$, $2b_2$, $1a_2$, $4a_1 \rightarrow np$, respectively. Due to the closely spaced *IP*s, the higher members of the Rydberg series are overlapped. Consequently only the first few members of each series are clearly distinguishable particularly in the case of *nd* series, where $n_{max}=6$ for $1a_2$ and $4a_1$ each and $n_{max}=5$ for $3b_1$ and $2b_2$ each could be identified. The quantum defect values obtained (c.f. Table 3) are in agreement with the atomic quantum defect values for *s*, *p* and *d* orbitals of Br, i.e., 2.96, 2.51 and 1.10, respectively [33].

Isotopic substitution is a well-known tool for confirming assignments in molecular spectra and it has been effectively used in several VUV photoabsorption studies reported recently [18–20]. In the present work, absorption spectrum of CD_2Br_2 is used to confirm and consolidate assignments. A comparison of the spectra of CH_2Br_2 and CD_2Br_2 (c.f. Fig. 2) shows that there exists an isotope shift of -180 to $+110\ cm^{-1}$ in the peak positions of Rydberg states. This variable shift may be understood by considering the difference in zero point energies of ground and excited states, which plays an important role in the assignment of the transitions. The expected position of the band origin under the harmonic approximation is given by $\nu_{00} = E' - E'' + (ZPE)' - (ZPE)''$, where single and double prime correspond to upper and lower state, *ZPE* is zero point energy given by $(\sum_{i=1}^{3N-6} \omega_i/2)$, ν_{00} is the band origin, *E* is equilibrium energy and ω_is are vibrational frequencies of the given electronic state. The main contribution to the isotopic shift is expected to arise from the difference in *ZPE*s of the two states involved. Now approximating excited state vibrational frequencies by ionic vibrational frequencies (see Table 2), we obtain approximately $200\ cm^{-1}$ as the magnitude of isotopic shift between CH_2Br_2 and CD_2Br_2. The variation of isotopic

Table 3
Rydberg series observed in VUV photoabsorption spectra of dibromomethane.[a]

Assignment	Experimentally observed in the present study						Previous study for CH_2Br_2 [16]
	CH_2Br_2			CD_2Br_2			
	Peak position		Q.D.	Peak position		Q.D.	Peak position (cm^{-1})
	cm^{-1}	eV		cm^{-1}	eV		
Converging to *IP* (b_1) = 10.52 eV (84,850 cm^{-1})							
$3b_1 \rightarrow 5s$	58,007	7.192	2.98	58,176	7.213	2.97	58,019
$3b_1 \rightarrow 6s$	72,452*	8.983	3.02	72,556	8.996	3.01	73,337
$3b_1 \rightarrow 7s$	78,005	9.671	3.00	78,007	9.672	3.00	78,779
$3b_1 \rightarrow 5p$	63,523	7.876	2.73	63,540	7.878	2.73	
$3b_1 \rightarrow 6p$	74,266	9.208	2.78	74,344	9.217	2.77	
$3b_1 \rightarrow 7p$	78,847*	9.776	2.72	78,832*	9.774	2.73	
$3b_1 \rightarrow 8p$	80,625*	9.996	2.90	80,662*	10.001	2.88	
$3b_1 \rightarrow 9p$	82,058*	10.174	2.73	82,113*	10.181	2.67	
$3b_1 \rightarrow 10p$	82,774*	10.263	2.73	82,821*	10.269	2.64	
$3b_1 \rightarrow 4d$	71,108	8.816	1.17	71,105	8.816	1.17	
$3b_1 \rightarrow 5d$	77,535	9.613	1.13	77,423	9.599	1.16	
Converging to *IP* (b_2) = 10.74 eV (86,820 cm^{-1})							
$2b_2 \rightarrow 5s$	59,510	7.378	2.99	59,689	7.400	2.98	59,511
$2b_2 \rightarrow 6s$	74,805	9.275	2.95	74,822	9.277	2.95	75,224
$2b_2 \rightarrow 7s$	79,294*	9.831	3.13	79,278	9.829	3.13	80,582
$2b_2 \rightarrow 8s$	82,058*	10.174	3.10	82,113*	10.181	3.07	82,976
$2b_2 \rightarrow 9s$	83,535	10.357	3.04	83,600	10.365	2.98	84,412
$2b_2 \rightarrow 5p$	65,778	8.155	2.71	65,813	8.160	2.70	
$2b_2 \rightarrow 6p$	76,124*	9.438	2.77	76,131*	9.439	2.77	
$2b_2 \rightarrow 7p$	80,625*	9.996	2.72	80,662*	10.001	2.71	
$2b_2 \rightarrow 4d$	72,452*	8.983	1.22	72,432	8.980	1.22	
$2b_2 \rightarrow 5d$	78,967	9.791	1.21	78,963	9.790	1.22	
Converging to *IP* (a_2) = 11.21 eV (90,410 cm^{-1})							
$1a_2 \rightarrow 5p$	68,668	8.514	2.75	68,716	8.520	2.75	
$1a_2 \rightarrow 6p$	79,294*	9.831	2.86	79,124	9.810	2.88	
$1a_2 \rightarrow 7p$	84,242*	10.445	2.78	84,237*	10.444	2.79	
$1a_2 \rightarrow 8p$	86,290	10.699	2.84	86,202*	10.688	2.90	
$1a_2 \rightarrow 4d$	75,266	9.332	1.31	75,441	9.353	1.29	
$1a_2 \rightarrow 5d$	82,774*	10.263	1.21	82,821*	10.269	1.20	
$1a_2 \rightarrow 6d$	85,573*	10.610	1.24	85,529*	10.604	1.26	
Converging to *IP* (a_1) = 11.30 eV (91,140 cm^{-1})							
$4a_1 \rightarrow 5s$	62,622	7.764	3.04	62,587	7.760	3.04	62,630
$4a_1 \rightarrow 6s$	78,847*	9.776	3.01	78,832*	9.774	3.01	77,956
$4a_1 \rightarrow 7s$	84,242*	10.445	3.01	84,237*	10.444	3.01	83,635
$4a_1 \rightarrow 5p$	69,362	8.600	2.76	69,265	8.588	2.76	
$4a_1 \rightarrow 6p$	81,291	10.079	2.66	81,322	10.083	2.66	
$4a_1 \rightarrow 7p$	85,573*	10.610	2.56	85,529*	10.604	2.58	
$4a_1 \rightarrow 8p$	87,347	10.830	2.62	87,319	10.826	2.64	
$4a_1 \rightarrow 9p$	88,400	10.960	2.67	88,384	10.958	2.69	
$4a_1 \rightarrow 4d$	76,124*	9.438	1.30	76,131*	9.439	1.30	
$4a_1 \rightarrow 5d$	82,976	10.288	1.33	83,016	10.293	1.32	
$4a_1 \rightarrow 6d$	86,129	10.679	1.32	86,202*	10.688	1.29	

[a] *Q.D.* – quantum defect value; *IP* – ionization potential and asterisks denote blended lines.

shift from state to state may be attributed to excited state vibrational frequencies being somewhat different from the calculated ionic frequencies. It may be noted that since the experimental resolution is ~50 cm^{-1} at 50,000 cm^{-1} and ~90 cm^{-1} at 90,900 cm^{-1}, shifts within these values are not really significant.

Vertical excitation energies, oscillator strengths and Λ diagnostic values predicted by PBE0/aug-cc-pV5Z level of theory along with experimental energies are listed in Table 4. The correspondence between theoretical and experimental data is established by taking into account the energies and symmetries of the initial and final MOs associated with every Rydberg member. This approach has been successfully used for assigning Rydberg levels in our earlier work [18]. It may be noted that in Table 4, we have shown only dipole allowed transitions up to ~11 eV. A complete list of vertical excited states can be provided by the authors on request. It is observed that most of the excited states of dibromomethane are predominantly Rydberg in nature as seen from the small Λ diagnostic values (c.f. Table 4). Also, the calculated and experimental energies are in overall good agreement for PBE0/aug-cc-pV5Z, the

Table 4
Vertical excitation energies, oscillator strengths and coefficients of wavefunctions for dominant transitions predicted by TDDFT using PBE0/aug-cc-pV5Z and comparison with experimentally observed transition energies of CH_2Br_2.

Sym	Transitions			Excitation energy (eV)	Oscillator strength	Λ[c]	Observed	
	Initial[a]	Final[a]	f[b]				Energy (eV)	Assignment
B_2	H-1($2b_2$)	L($5a_1$)	0.99	5.598	< 0.001	0.6	~5.6[d]	
B_1	H($3b_1$)	L($5a_1$)	0.97	5.671	0.029	0.6		
A_1	H-3($4a_1$)	L($5a_1$)	0.96	6.154	0.001	0.6	~6.3[d]	
A_1	H($3b_1$)	L+2($4b_1$)	0.94	6.808	0.007	0.5		
B_1	H($3b_1$)	L+1($6a_1$)	−0.95	7.025	0.043	0.3	7.192	$3b_1 \rightarrow 5s$
B_2	H-1($2b_2$)	L+1($6a_1$)	0.91	7.052	0.059	0.3	7.378	$2b_2 \rightarrow 5s$
B_2	H-2($1a_2$)	L+2($4b_1$)	0.9	7.304	<0.001	0.4	~7.7[d]	
B_1	H-3($4a_1$)	L+2($4b_1$)	0.9	7.572	0.159	0.5		
A_1	H-3($4a_1$)	L+1($6a_1$)	0.96	7.609	0.027	0.3	7.764	$4a_1 \rightarrow 5s$
A_1	H-1($2b_2$)	L+3($3b_2$)	−0.98	7.847	0.010	0.2	8.155	$2b_2 \rightarrow 5p$
B_1	H($3b_1$)	L+4($7a_1$)	0.98	8.017	0.001	0.2	7.876	$3b_1 \rightarrow 5p$
B_2	H-1($2b_2$)	L+4($7a_1$)	0.98	8.089	0.047	0.3	8.983	$2b_2 \rightarrow 4d$
A_1	H($3b_1$)	L+5($5b_1$)	−0.93	8.169	0.019	0.4	~8.3[d]	
B_1	H-2($1a_2$)	L+3($3b_2$)	−0.97	8.240	0.024	0.2	8.514	$1a_2 \rightarrow 5p$
B_2	H-3($4a_1$)	L+3($3b_2$)	0.96	8.340	< 0.001	0.1	8.600	$4a_1 \rightarrow 5p$
B_2	H-2($1a_2$)	L+5($5b_1$)	−0.81	8.525	0.015	0.3	~8.3[d]	
A_1	H-3($4a_1$)	L+4($7a_1$)	0.91	8.578	0.023	0.3	~8.3[d]	
B_1	H($3b_1$)	L+6($8a_1$)	−0.88	8.591	0.023	0.3	8.983	$3b_1 \rightarrow 6s$
B_1	H-3($4a_1$)	L+5($5b_1$)	0.81	8.672	0.031	0.3	9.438	$4a_1 \rightarrow 4d$
B_2	H-1($2b_2$)	L+6($8a_1$)	−0.86	8.698	0.037	0.3	9.275	$2b_2 \rightarrow 6s$
A_1	H($3b_1$)	L+7($6b_1$)	0.9	8.886	0.029	0.3	9.208	$3b_1 \rightarrow 6p$
B_2	H($3b_1$)	L+10($2a_2$)	−0.95	8.957	0.008	0.2	8.816	$3b_1 \rightarrow 4d$
A_1	H-1($2b_2$)	L+8($4b_2$)	−0.94	8.982	0.005	0.3	9.438	$2b_2 \rightarrow 6p$
B_1	H($3b_1$)	L+9($9a_1$)	−0.81	8.991	0.003	0.3	9.671	$3b_1 \rightarrow 7s$
B_1	H-1($2b_2$)	L+10($2a_2$)	−0.79	9.039	0.128	0.3	9.791	$2b_2 \rightarrow 5d$
B_2	H-1($2b_2$)	L+9($9a_1$)	−0.93	9.060	0.002	0.2	9.831	$2b_2 \rightarrow 7s$
A_1	H-3($4a_1$)	L+6($8a_1$)	−0.94	9.195	0.027	0.3	~9.1[d]	
B_1	H($3b_1$)	L+11($10a_1$)	−0.65	9.214	0.008	0.4	~9.1[d]	
	H-4($2b_1$)	L($5a_1$)	0.555					
B_1	H($3b_1$)	L+11($10a_1$)	−0.66	9.290	0.073	0.3	~9.1[d]	
	H-2($1a_2$)	L+8($4b_2$)	−0.55				9.332	$1a_2 \rightarrow 4d$
B_2	H-1($2b_2$)	L+11($10a_1$)	0.98	9.305	0.001	0.3	10.174	$2b_2 \rightarrow 8s$
B_2	H-2($1a_2$)	L+7($6b_1$)	0.96	9.335	0.001	0.2	9.831	$1a_2 \rightarrow 6p$
B_1	H-3($4a_1$)	L+7($6b_1$)	0.72	9.409	0.056	0.3	10.079	$4a_1 \rightarrow 6p$
	H-2($1a_2$)	L+8($4b_2$)	0.59				~9.6[d]	
A_1	H-2($1a_2$)	L+10($2a_2$)	0.65	9.413	0.001	0.3	~9.6[d]	
B_2	H-3($4a_1$)	L+8($4b_2$)	0.94	9.455	0.027	0.2	10.288	$4a_1 \rightarrow 5d$
A_1	H-1($2b_2$)	L+12($5b_2$)	−0.86	9.456	0.010	0.2	9.996	$2b_2 \rightarrow 7p$
A_1	H-3($4a_1$)	L+9($9a_1$)	0.57	9.543	0.014	0.3	9.776	$4a_1 \rightarrow 6s$
	H($3b_1$)	L+13($7b_1$)	0.53				9.613	$3b_1 \rightarrow 5d$
	H-2($1a_2$)	L+10($2a_2$)	−0.58				~9.6[d]	
B_1	H($3b_1$)	L+14($11a_1$)	−0.57	9.596	0.022	0.4	~9.6[d]	
	H-4($2b_1$)	L($5a_1$)	0.461					
A_1	H($3b_1$)	L+13($7b_1$)	−0.72	9.650	0.005	0.2	9.776	$3b_1 \rightarrow 7p$
	H-3($4a_1$)	L+9($9a_1$)	0.67				10.445	$4a_1 \rightarrow 7s$
A_1	H-3($4a_1$)	L+11($10a_1$)	−0.9	9.825	0.005	0.3	10.610	$4a_1 \rightarrow 7p$
B_1	H-2($1a_2$)	L+12($5b_2$)	0.84	9.847	0.004	0.2	10.263	$1a_2 \rightarrow 5d$
B_2	H-1($2b_2$)	L+14($11a_1$)	0.97	9.852	0.024	0.3	10.357	$2b_2 \rightarrow 9s$
B_1	H($3b_1$)	L+14($11a_1$)	0.7	9.866	0.112	0.3	9.996	$3b_1 \rightarrow 8p$
	H-2($1a_2$)	L+12($5b_2$)	−0.49				10.445	$1a_2 \rightarrow 7p$
A_1	H-5($3a_1$)	L($5a_1$)	−0.77	9.881	0.024	0.6	~10.0[d]	
B_2	H-3($4a_1$)	L+12($5b_2$)	−0.96	9.948	<0.001	0.2	10.679	$4a_1 \rightarrow 6d$
A_1	H-1($2b_2$)	L+15($6b_2$)	−0.81	10.038	0.002	0.5	~10.0[d]	
B_2	H-2($1a_2$)	L+13($7b_1$)	−0.97	10.065	0.034	0.2	10.610	$1a_2 \rightarrow 6d$
B_1	H-3($4a_1$)	L+13($7b_1$)	0.97	10.146	0.013	0.2	10.830	$4a_1 \rightarrow 8p$
A_1	H($3b_1$)	L+16($8b_1$)	0.89	10.288	0.021	0.3	10.174	$3b_1 \rightarrow 9p$
B_2	H-3($4a_1$)	L+15($6b_2$)	−0.9	10.398	0.001	0.4	~10.3[d]	
A_1	H-3($4a_1$)	L+14($11a_1$)	−0.88	10.405	0.054	0.3	10.960	$4a_1 \rightarrow 9p$
B_1	H-2($1a_2$)	L+15($6b_2$)	−0.86	10.408	0.144	0.4	~10.3[d]	
B_2	H($3b_1$)	L+17($3a_2$)	0.89	10.524	0.016	0.3	[e]	
B_1	H-1($2b_2$)	L+17($3a_2$)	−0.65	10.573	0.005	0.4	~10.8[d]	
B_1	H-4($2b_1$)	L+1($6a_1$)	0.811	10.584	0.031	0.3	10.263	$3b_1 \rightarrow 10p$
B_2	H-2($1a_2$)	L+16($8b_1$)	−0.95	10.797	0.105	0.3	10.699	$1a_2 \rightarrow 8p$
A_1	H-4($2b_1$)	L+2($4b_1$)	−0.62	10.823	0.007	0.5	~10.8[d]	
	H-2($1a_2$)	L+17($3a_2$)	0.57					

Table 4 (*continued*)

Sym	Transitions			Excitation energy (eV)	Oscillator strength	Λ[c]	Observed	
	Initial[a]	Final[a]	f[b]				Energy (eV)	Assignment
B_1	H-3($4a_1$)	L+16($8b_1$)	−0.81	10.864	0.050	0.3	[e]	
B_1	H-5($3a_1$)	L+2($4b_1$)	0.61	10.888	0.290	0.4	~10.8[d]	
B_2	H-6($1b_2$)	L($5a_1$)	−0.93	10.918	0.003	0.5	~10.8[d]	
B_1	H($3b_1$)	L+18($12a_1$)	0.91	10.991	0.149	0.3	[e]	
B_2	H-1($2b_2$)	L+18($12a_1$)	−0.91	11.062	0.067	0.4	~10.8[d]	

[a] H and L are highest occupied and lowest unoccupied molecular orbitals, respectively.
[b] Excitation amplitude.
[c] Value of Λ diagnostic.
[d] Valence transitions.
[e] Expected but unresolved Rydberg transitions.

difference is within 0.9 eV. It may be noted that the agreement between theoretical and experimental values is better for relatively low-lying excited states as expected, whereas for higher excited states (close to ionization limits) interactions among the various states make it difficult to correspond the experimentally observed and theoretical values with a high degree of confidence.

Based on the quantum defect analysis (c.f. Table 3), the three transitions at 58,007, 59,510 and 62,622 cm^{-1} (7.192, 7.378 and 7.764 eV) are identified as corresponding to excitations $3b_1$, $2b_2$, $4a_1 \rightarrow 5s$, respectively, in agreement with the assignment of the bands at 58,019, 59,511, and 61,995 cm^{-1} by Causley and Russell [16]. These transitions are assigned to theoretically predicted energies at 7.025, 7.052 and 7.609 eV (c.f. Table 4) based on the nature of orbital excitation. Following this logic, the higher members of *ns* Rydberg series for $n=6$, identified with excitations from $3b_1$, $2b_2$, $4a_1 \rightarrow 6s$ are predicted at 8.591, 8.698 and 9.543 eV and are observed experimentally at 72,452, 74,805 and 78,847 cm^{-1} (8.982, 9.275 and 9.776 eV), respectively. Transitions corresponding to excitations $3b_1$, $2b_2$, $4a_1 \rightarrow 7s$ are calculated to be at 8.991, 9.060 and 9.650 eV and they correspond to experimentally observed transitions at 78,005, 79,294 and 84,242 cm^{-1} (9.671, 9.831 and 10.445 eV), respectively. Higher *ns* series members ($n > 7$) are observed in our experiments only for $2b_2$, but not for $3b_1$ and $4a_1$. The observed transitions at 82,058 and 83,535 cm^{-1} (10.174 and 10.357 eV) corresponding to $2b_2 \rightarrow 8s$ and $2b_2 \rightarrow 9s$ are predicted at 9.305 and 9.852 eV, respectively.

Using the same approach, the correspondence of experimentally observed *np* and *nd* Rydberg series with theoretically predicted transitions is carried out. Considering excitations $3b_1$, $2b_2$, $4a_1$, $1a_2 \rightarrow np$, *nd* and keeping in mind that the transition $b_1 \leftrightarrow b_2$ is forbidden under C_{2v} symmetry, experimentally observed members of *np* and *nd* series converging to all four *IP*s could be assigned to TDDFT predicted vertical excited states. Note that in the present analysis, we have considered only those excitations for which the absolute value of TDDFT excitation amplitude is ≥ 0.5. It is observed that most of the predicted excited states are dominated by a single excitation with high coefficient (> 0.9) whereas mixing of a few excitations with lower coefficient (0.6-0.9) may be seen for some of the excited states. All the members of Rydberg series (*ns*, *np* and *nd*) corresponding to Br non-bonding orbitals could be assigned to the transitions predicted by TDDFT (c.f. Table 4).

Based on term value calculations Causley and Russell [16] assigned the b_1, b_2, $(a_1+a_2) \rightarrow 5p$, $4d$ transitions, i.e., first members of *np* and *nd* series, but did not assign higher members of these series. In our work we observe higher members of *np* and *nd* Rydberg series. As regards the assignments of ns series, our assignment differs from those of Causley and Russell [16] in some places, for instance, the peaks 77,956, 83,635, 78,779 and 82,976 cm^{-1} assigned by them to $4a_1 \rightarrow 6s$, $4a_1 \rightarrow 7s$, $3b_1 \rightarrow 7s$ and $2b_2 \rightarrow 8s$ are reassigned in our work to $3b_1 \rightarrow 7s$, $2b_2 \rightarrow 9s$, $4a_1 \rightarrow 6s$ and $4a_1 \rightarrow 5d$, respectively. The peak reported earlier [16] at 80,582 cm^{-1} for the transition $2b_2 \rightarrow 7s$ is found in the present study to belong to blended transitions $3b_1 \rightarrow 8p$ and $2b_2 \rightarrow 7p$ at 80,625 cm^{-1}. The peak observed by Causley and Russell [16] at 84,412 cm^{-1} has appeared as a weak shoulder in our spectrum while the clearer peak at 84,242 cm^{-1} (c.f. Fig. 2) was not reported by them. The $3b_1 \rightarrow 6s$ transition assigned by them at 73,337 cm^{-1} is observed in the present study at 72,452 cm^{-1} consisting of blended transitions $3b_1 \rightarrow 6s$ and $3b_2 \rightarrow 4s$. It may be noted that Causley and Russell used only three values of *IP*s 10.61, 10.82 and 11.28 eV corresponding to b_1, b_2 and (a_1+a_2) as known at that time in literature. Recently, from advanced experimental techniques [5,13] the values of *IP*s for $1a_2$ and $4a_1$ are distinguishably known (11.21 and 11.30 eV) together with more precise values of the other *IP*s. In the present study, the availability of precise values of *IP*s of CH_2Br_2 and the spectrum of its deuterated isotopologue (CD_2Br_2) has resulted in successful identification and assignment of Rydberg series converging to all four *IP*s. Further, the comparative study of two isotopic species helped in assigning a few transitions which are not well resolved for one of the isotopic species but resolved clearly in the other. For example, transitions $3b_1 \rightarrow 6s$ and $2b_2 \rightarrow 4d$ blended at 72,452 cm^{-1} in CH_2Br_2 are resolved at 72,556 and 72,432, respectively, for CD_2Br_2. Similarly the peak observed at 79,293 cm^{-1} corresponding to $2b_2 \rightarrow 7s$ and $1a_2 \rightarrow 6p$ for CH_2Br_2 appears distinctly at 79,278 and 79,124 cm^{-1} in CD_2Br_2. Transitions $1a_2 \rightarrow 8p$ and $4a_1 \rightarrow 6d$ at 86,290 and 86,129 cm^{-1}, respectively, are resolved in CH_2Br_2 which are blended in CD_2Br_2 at 86,202 cm^{-1}. A

Table 5
Vibrational features observed in VUV photoabsorption spectra of dibromomethane.

Present study					Previous study for CH_2Br_2 [16]	
Assignment	Peak position				Position (cm^{-1})	Assignment
	CH_2Br_2		CD_2Br_2			
	cm^{-1}	eV	cm^{-1}	eV		
$3b_1 \rightarrow 5p+\nu_3$	64,310	7.973	64,344	7.978	64,310	$4p(b_1) \rightarrow 5p+\nu_3$
$3b_1 \rightarrow 5p+2\nu_3$	65,018	8.061	65,088	8.070	65,063	$4p(b_1) \rightarrow 5p+\nu_2$
$3b_1 \rightarrow 5p+3\nu_3$	65,778	8.155	65,813	8.160		
$2b_2 \rightarrow 5p+\nu_3$	66,518	8.247	66,539	8.250	66,495	$4p(b_2) \rightarrow 5p+\nu_3$
$2b_2 \rightarrow 5p+2\nu_3$	67,235	8.336	67,353	8.351	67,233	$4p(b_2) \rightarrow 5p+\nu_2$
$1a_2 \rightarrow 5p+\nu_3$	69,362	8.600	69,265	8.588	69,330	$4p(a_1+a_2) \rightarrow 5p+\nu_3$
$3b_1 \rightarrow 4d+\nu_3$	71,747	8.895	71,686	8.888		
$3b_1 \rightarrow 4d+2\nu_3$	72,327	8.967	72,316	8.966		
$2b_2 \rightarrow 4d+\nu_3$	–	–	72,963	9.046		
$2b_2 \rightarrow 4d+2\nu_3$	73,669	9.134	73,668	9.134		

comparative study of CD_2Br_2 and CD_2Br_2 thus has served well to resolve uncertainties such as these.

4.2. Vibronic assignments

The Rydberg transition $3b_1 \rightarrow 5p$ (63,523 cm^{-1}) of CH_2Br_2 is accompanied by vibronic peaks at 64,310, 65,018, 65,778 cm^{-1} (c.f. Fig. 2) at intervals of ~787, 1495 and 2255 cm^{-1}. Causley and Russell [16] assigned the first two peaks to the totally symmetrical modes ν_3 and ν_2, respectively, since these two intervals match with the vibrational frequencies of these two modes in the ground state. These peaks are observed at 64,344, 65,088 and 65,813 cm^{-1} with intervals 804, 1548 and 2273 cm^{-1} from the origin 63,540 cm^{-1} in CD_2Br_2 spectrum. Isotopic shift in the peak positions is found to be very small (< 70 cm^{-1}). Assignment of the band at 65,018 cm^{-1} to the ν_2 (–CH_2 bend) mode is ruled out on the basis of the observation that the frequency of ν_2 changes from 1382 to 1027 cm^{-1} in going from CH_2Br_2 to CD_2Br_2 in the ground state (c.f. Table 2) and a similar trend is expected in the excited state. Relative insensitivity to deuterium substitution suggests that the vibrational mode contributing to these peaks should involve the -CBr_2 group. Therefore, we assign these three peaks to the progression of $n\nu_3$ ($n=1$, 2 and 3) of $3b_1 \rightarrow 5p$ Rydberg state. Using the same logic, bands at 66,518 and 67,235 cm^{-1} of CH_2Br_2 observed at 66,539 and 67,353 cm^{-1} in CD_2Br_2 can be assigned to $n\nu_3$ ($n=1$ and 2) of $3b_2 \rightarrow 5p$ Rydberg state in contrast to the earlier study [16] where they are assigned to ν_3 and ν_2 modes, respectively. It should be noted that the peak at 69,265 cm^{-1} (blue shifted by ~550 cm^{-1} from 68,716 cm^{-1}) in CD_2Br_2 spectrum is sharp and it is assigned to $4a_1 \rightarrow 5p$ transition on the basis of quantum defect value. In case of CH_2Br_2 we observe that the same transition at 69,362 cm^{-1} is broad and the vibrational mode $1a_2 \rightarrow 5p+\nu_3$ may be coinciding with Rydberg transition $4a_1 \rightarrow 5p$ which is consistent with the earlier assignment [16]. Similarly peaks observed in CH_2Br_2 (CD_2Br_2) at 71,747 (71,686) and 72,327 (72,316) cm^{-1} are assigned to ν_3 of $3b_1 \rightarrow 4d$ Rydberg state. Peaks of CD_2Br_2 at 72,963 and 73,668 cm^{-1} are assigned to ν_3 ($n=1$ and 2) of $3b_2 \rightarrow 4d$ Rydberg state. In this case, $n=1$ component is not resolved in the CH_2Br_2 spectrum and $n=2$ component appears at 73,669 cm^{-1}. Table 5 shows vibronic assignments for CH_2Br_2 and CD_2Br_2 in the present study and comparison with previous assignments for CH_2Br_2. Here it is worth mentioning that the spectrum of CD_2Br_2 in the present study plays an important role in confirming all the above vibronic assignments to excitation of the ν_3 mode alone instead of ν_3 and ν_2 as suggested by Causley and Russell [16].

From the above assignments, the values of excited state vibrational frequencies of –CBr symmetrical stretching mode (ν_3) in CH_2Br_2 (CD_2Br_2) are estimated to be 753 (766), 731 (761), 694 (549), 615 (601) and 609 (601) cm^{-1} for $3b_1 \rightarrow 5p$, $3b_2 \rightarrow 5p$, $1a_2 \rightarrow 5p$, $3b_1 \rightarrow 4d$ and $3b_2 \rightarrow 4d$, respectively, within an error of ± 15 cm^{-1}. The broad and irregular intensity pattern of the vibronic bands may suggest contributions due to perturbations from other states and from hot/sequence bands involving the low-frequency ν_4 mode.

4.3. Valence transitions

In the regions 4.3–6.7 eV two broad humps centered at 45,000 and 51,000 cm^{-1} are observed at high (~1 mbar) sample pressure (inset of Fig. 2). These are earlier reported at 45,590 and 51,490 cm^{-1} by Causley and Russell [16]. These features are also reported by Ito et al. in CH_2Br_2 solution spectrum [34]. The lower energy band was tentatively assigned to $n(b_2) \rightarrow \sigma^*$ and $n(b_1) \rightarrow \sigma^*$ while the higher energy band was proposed to be composed of contributions from $n(a_1) \rightarrow \sigma^*$ and $n(b_2+b_1) \rightarrow \sigma^{**}$ [16]. Later, on the basis of spin orbit ab initio investigations, Liu et al. assigned these two bands to 4^1B_1 and 5^1A_1 states, respectively [15]. It is evident from the TDDFT calculations (c.f. Table 4) that the first four vertical excited states lying in 5.6–6.8 eV region and having nonzero oscillator strength correspond to excitation from Br nonbonding orbitals ($2b_2$, $3b_1$, $4a_1$) $\rightarrow 5a_1$ and $3b_1 \rightarrow 4b_1$. These states exhibit valence character as evident from the relatively high values of Λ (0.6 and 0.5). We therefore assign the lower energy band (45,000 cm^{-1}) to the transitions

$2b_2$, $3b_1 \rightarrow 5a_1$ in agreement with the assignment of Ito et al. [34]. Of these two transitions, the major contribution to intensity is expected from $3b_1 \rightarrow 5a_1$ owing to higher oscillator strength (0.03). The higher energy band at 51,000 cm^{-1} may be assigned to the transitions $4a_1 \rightarrow 5a_1$ and $3b_1 \rightarrow 4b_1$ with calculated energies of 6.8 eV and 7.0 eV and oscillator strengths of 0.001 and 0.007, respectively.

In the energy region of 6.8–7.8 eV, four broad absorption features (58,007, 59,510, 61,995 and 62,622 cm^{-1}) are observed in contrast to three in the earlier study [16]. Of these, the three peaks at 58,007, 59,510 and 62,622 cm^{-1} are assigned to 5*s* Rydberg states as discussed in Section 4.1. The additional peak observed at 61,995 cm^{-1} may be assigned to the TDDFT predicted valence transitions $1a_2$, $4a_1 \rightarrow 4b_1$ at 7.030 eV ($\Lambda = 0.4$) and 7.512 eV ($\Lambda = 0.4$), respectively; the latter transition with calculated oscillator strength of 0.16 is most likely to be the main contributor to the intensity.

In the higher energy region (> 7.8 eV), the Rydberg features appear on a broad intensity pedestal and in fact several of them appear. Causley and Russell [16] proposed that the high underlying intensity could be due to the presence of valence states and three $\sigma \rightarrow \sigma^*$ transitions contributing to the underlying intensity around 9.1, 9.7 and 10.4 eV. A close scrutiny of the spectrum (c.f. Fig. 2) shows six regions centered around ~8.3, 9.1, 9.6, 10.0, 10.3 and 10.7 eV. Interestingly, these essentially correspond to the TDDFT predicted transitions that are not assigned to any Rydberg transition (c.f. Table 4). We expect these transitions have valence character and as may be seen from Table 4 that most of these have higher Λ values. These valence transitions are responsible for exhibiting broad underlying intensity in the above identified regions. For example, the transitions $3b_1, 1a_2 \rightarrow 5b_1$ and $4a_1 \rightarrow 7a_1$ at 8.169, 8.525 and 8.578 eV, respectively, are likely to contribute to the background intensity around 8.3 eV. Similarly, the valence transitions $4a_1 \rightarrow 8a_1$, $3b_1 \rightarrow 10a_1$ and $2b_1 \rightarrow 5a_1$ appear to be responsible for the underlying intensity around 9.1 eV. Analogous inferences can be drawn for the other intensity regions, i.e., 9.6, 10.0, 10.3 and 10.7 eV. Finally we may point out that in Table 4 a few excited states calculated at 9.6, 10.0, 10.3 and 10.7 eV exhibit mixed valence–Rydberg character, i.e., one of the components is assigned to a Rydberg transition while the other is expected to behave as a valence transition.

5. Conclusions

We have reported here the photoabsorption spectrum of dibromomethane in the energy region of4.3–11.8 eV obtained using synchrotron radiation. The spectrum is dominated by Rydberg series converging to first four ionization potentials, i.e., 10.52, 10.74, 11.21 and 11.30 eV. Quantum defect analysis is used to assign *ns*, *np* and *nd* Rydberg series originating from the four outermost ($3b_1$, $2b_2$, $1a_2$, $4a_1$) orbitals of CH_2Br_2. The analysis is further supported using quantum chemical calculations at the PBE0/aug-cc-pV5Z level, which provide an overall good agreement with the experimental values. Earlier assignments of *ns* series are revised, and *np* and *nd* Rydberg series are assigned for the first time. The underlying intensity in the photoabsorption spectrum is attributed to valence or valence–Rydberg mixed type transitions as obtained from TDDFT calculations. Observed vibrational features associated with 5*p* and 4*d* Rydberg states are assigned to the totally symmetric (a_1) –CBr symmetric stretching mode (ν_3) of $3b_1$, $3b_2$, $1a_2 \rightarrow 5p$ and $3b_1$, $3b_2 \rightarrow 4d$ Rydberg states in contrast to the earlier assignments of ν_3 and $-CH_2$ bending (ν_2). Proposed assignments are confirmed by the UV–VUV photoabsorption spectrum of dibromomethane-d_2 (CD_2Br_2) whose spectrum is reported here for the first time. This work presents a consolidated analysis of the UV–VUV photoabsorption spectrum of dibromomethane.

Acknowledgment

Authors thank Drs. S.N. Jha and N.K. Sahoo for their interest and support.

References

[1] Goodwin KD, Lidstrom ME, Oremland RS. Marine bacterial degradation of brominated methanes. Environ Sci Technol 1997;31:3188–92.
[2] Mossinger JC, Shallcross DE, Cox. RA. UV–vis absorption cross-sections and atmospheric lifetimes of CH_2Br_2, CH_2I_2 and CH_2BrI. J Chem Soc, Faraday Trans 1998;94:1391–6.
[3] Molina LT, Molina MJ, Rowland FS. Ultraviolet absorption cross sections of several brominated methanes and ethanes of atmospheric interest. J Phys Chem 1982;86:2672–6.
[4] Liang Q, Stolarski RS, Kawa SR, Nielsen JE, Douglass AR, Rodriguez JM, et al. Finding the missing stratospheric Bry: a global modeling study of $CHBr_3$ and CH_2Br_2. Atmos Chem Phys 2010;10:2269–86.
[5] Lago AF, Kercher JP, Bodi A, Sztáray B, Miller B, Wurzelmann D, et al. Dissociative photoionization and thermochemistry of dihalomethane compounds studied by threshold photoelectron photoion coincidence spectroscopy. J Phys Chem A 2005;109:1802–9.
[6] Tsai BP, Baer T, Werner AS, Lin SF. Photoelectron–photoion coincidence study of the ionization and fragment appearance potentials of bromo- and iodomethanes. J Phys Chem 1975;79:570–4.
[7] Huang J, Xu D, Fink WH, Jackson WM. Photodissociation of the dibromomethane cation at 355 nm by means of ion velocity imaging. J Chem Phys 2001;115:6012–7.
[8] Ji L, Tang Y, Zhu R, Wei Z, Zhang B. Photodissociation dynamics of CH_2Br_2 near 234 and 267 nm. Spectrochim Acta Part A: Mol Biomol Spectrosc 2007;67:273–80.
[9] Ji L, Tang Y, Zhu R, Tang B, Zhang B. Studies on photodissociation of dibromoalkane in UV region. Chem Phys 2005;314:173–8.
[10] Sharma P, Vatsa RK, Maity DK, Kulshreshtha SK. Laser induced photodissociation of CH_2Cl_2 and CH_2Br_2 at 355 nm: an experimental and theoretical study. Chem Phys Lett 2003;382:637–43.
[11] Wei P-Y, Chang Y-P, Lee W-B, Hu Z, Huang H-Y, Lin K-C, et al. 248 nm photolysis of CH_2Br_2 by using cavity ring-down absorption spectroscopy: Br_2 molecular elimination at room temperature. J Chem Phys 2006;125:133319.
[12] Dixon RN, Murrell JN, Narayan B. The photoelectron spectra of the halomethanes. Mol Phys 1971;20:611–23.
[13] Kishimoto N, Matsumura E, Ohno K, Deleuze MS. Collision-energy-resolved Penning ionization electron spectroscopy of bromomethanes (CH_3Br,CH_2Br_2, and $CHBr_3$) by collision with $He^*(23S)$ metastable atoms. J Chem Phys 2004;121:3074–86.
[14] Gillotay D, Simon PC. Ultraviolet absorption cross-sections of photoactive species of stratospheric interest. Part 1: halocarbons. Aeron Acta A 1990;356:1–173.
[15] Liu Y, Xiao H, Sun M, Fang W. Spin–orbit ab initio investigation of the photodissociation of dibromomethane in the gas and solution phases. J Comput Chem 2008;29:2513–9.
[16] Causley GC, Russell BR. Vacuum ultraviolet absorption spectra of the bromomethanes. J Chem Phys 1975;62:848–57.
[17] Das NC, Raja Sekhar BN, Saraswathy P, Shastri A, Bhattacharya SS, Bhatt S, et al. Development of photophysics beamline at Indus-1 synchrotron radiation source. J Opt 2003;32:169–76.

[18] Singh PJ, Shastri A, D'Souza R, Jagatap BN. Rydberg states of chloroform studied by VUV photoabsorption spectroscopy. J Quant Spectrosc Radiat Transf 2013;129:204–13.
[19] Shastri A, Singh PJ, Raja Sekhar BN, D'Souza R, Jagatap BN. The role of torsional modes in the electronic absorption spectrum of acetone. J Quant Spectrosc Radiat Transf 2012;113:1553–65.
[20] Singh PJ, Shastri A, Raja Sekhar BN, D'Souza R, Jagatap BN. Effect of isotopic substitution in the electronic absorption spectrum of acetone: VUV photoabsorption studies of acetone-d6. J Quant Spectrosc Radiat Transf 2013;114:20–8.
[21] Schmidt MW, Baldridge KK, Boatz JA, Elbert ST, Gordon MS, Jensen JH, et al. General atomic and molecular electronic structure system. J Comput Chem 1993;14:1347–63.
[22] Becke AD. Density-functional thermochemistry. III. The role of exact exchange. J Chem Phys 1993;98:5648–52.
[23] Lee C, Yang W, Parr RG. Development of the Colle–Salvetti correlation-energy formula into a functional of the electron density. Phys Rev B 1988;37:785–9.
[24] Perdew JP, Burke K, Ernzerhof M. Generalized gradient approximation made simple. Phys Rev Lett 1996;77:3865–8.
[25] Francl MM, Pietro WJ, Hehre WJ, Binkley JS, Gordon MS, DeFrees DJ, et al. Self-consistent molecular orbital methods. XXIII. A polarization-type basis set for second-row elements. J Chem Phys 1982;77:3654–65.
[26] Frisch MJ, Pople JA, Binkley JS. Self-consistent molecular orbital methods 25. Supplementary functions for Gaussian basis sets. J Chem Phys 1984;80:3265–9.
[27] Dennen RS, Piotrowski EA, Cleveland FF. Raman and infrared spectral data for CH_2Br_2, $CHDBr_2$, and CD_2Br_2. J Chem Phys 1968;49:4385–91.
[28] K.G.G. Kuchitsu. Structure of free polyatomic molecules: basic data. Berlin, New York: Springer; 1998.
[29] Venkatraman R, Kwiatkowski JS, Bakalarski G, Leszczynski J. Molecular structure and IR spectra of bromomethanes by DFT and post-Hartree–Fock MP2 and CCSD(T) calculations. Mol Phys 2000;98:371–86.
[30] Kisiel Z, Kraśnicki A, Pszczółkowski L, Shipman ST, Alvarez-Valtierra L, Pate BH. Assignment and analysis of the rotational spectrum of bromoform enabled by broadband FTMW spectroscopy. J Mol Spectrosc 2009;257:177–86.
[31] Peach MJG, Benfield P, Helgaker T, Tozer DJ. Excitation energies in density functional theory: an evaluation and a diagnostic test. J Chem Phys 2008;128:044118-1–8.
[32] Potts AW, Lempka HJ, Streets DG, Price WC. Photoelectron spectra of the halides of elements in groups III, IV, V and VI. Philos Trans R Soc Lond Ser A: Math Phys Sci 1970;268:59–76.
[33] Theodosiou CE, Inokuti M, Manson ST. Quantum defect values for positive atomic ions. Atomic Data Nucl Data Tables 1986;35:473–86.
[34] Ito M, Huang P-kC, Kosower EM. Electronic absorption spectra of iodo- and bromomethanes. Trans Faraday Soc 1961;57:1662–73.